Bloch Oscillations, Zener Tunneling, and Wannier-Stark Ladders in the Time Domain

Rotvig, Jon; Jauho, Antti-Pekka; Smith, Henrik

Published in:
Physical Review Letters

Link to article, DOI:
10.1103/PhysRevLett.74.1831

Publication date:
1995

Document Version
Publisher's PDF, also known as Version of record

Bloch Oscillations, Zener Tunneling, and Wannier-Stark Ladders in the Time Domain

Jon Rotvig,[1] Antti-Pekka Jauho,[2] and Henrik Smith[1]

[1]*Ørsted Laboratory, H.C. Ørsted Institute, Universitetsparken 5, University of Copenhagen, DK-2100 Copenhagen Ø, Denmark*

[2]*Mikroelektronik Centret, Technical University of Denmark, DK-2800 Lyngby, Denmark*

(Received 25 October 1994)

We present a time-domain analysis of carrier dynamics in a semiconductor superlattice with two minibands. Integration of the density-matrix equations of motion reveals a number of new features: (i) for certain values of the applied static electric field strong interminiband transitions occur; (ii) in static fields the complex time dependence of the density matrix displays a sequence of stable plateaus in the low field regime, and (iii) for harmonic fields the Fourier representation of the density matrix is shown to be intimately related to the quasienergy spectrum.

PACS numbers: 73.20.Dx, 73.40.Gk, 73.50.Fq

Bloch oscillations (BO) are one of the most striking predictions of the semiclassical theory of electronic transport: In any system of independent electrons in a periodic potential the electron velocity becomes a periodic function of time with characteristic frequency $\omega_B = eEd/\hbar$, where d is the lattice period and E is the applied field [1]. In ordinary bulk materials these oscillations cannot be seen, because collisions dephase the coherent motion of electrons on a time scale which is much shorter than $T_B = 2\pi/\omega_B$. However, as pointed out by Esaki and Tsu [2], the conditions for observing BO's are much less stringent for high-quality semiconductor superlattices. Recent years have witnessed an intense experimental activity in this area, culminating in the observation of terahertz radiation from coherently oscillating electrons [3].

There has been equal activity on the theoretical side. Holthaus [4] analyzed the semiclassical motion of electrons in a single miniband subjected to a strong *alternating* electric field. Studies of this kind have gained importance due to the emerging free-electron lasers [5], which open the possibility of experimental probing of the theoretical predictions. For certain values of the system parameters a dynamical localization takes place [6]: the average velocity vanishes. This phenomenon can alternatively be called band collapse [4]. Analogies between the Josephson effect and electronic motion in periodic potentials have been discussed several times [7]. Very recently, Meier *et al.* [8] considered coherent motion of photoexcited carriers in the presence of Coulomb interaction, and found out that BO's should persist even in the limit where the exciton binding energy is comparable to the miniband width.

The papers quoted above have mainly concentrated on studying systems with one miniband [9]; the central theme in the present work is to study the dynamics of electrons in a *two-band* superlattice. The second miniband adds an essential feature to the model: It is possible to study how Zener tunneling affects the dynamics of the carriers. Our method consists of setting up, and solving, the density-matrix equations of motion for the two-band system. In this paper we focus on the coherent part of the motion. This coherent motion displays in its own right a number of interesting features, which we shall describe after having sketched the general formalism.

First we need to define the microscopic model underlying the density matrix calculation. The model Hamiltonian is

$$H = \sum_n \Big[(\Delta_0^a + neEd) a_n^\dagger a_n + (\Delta_0^b + neEd) b_n^\dagger b_n - \frac{\Delta_1^a}{4}(a_{n+1}^\dagger a_n + a_n^\dagger a_{n+1}) + \frac{\Delta_1^b}{4}(b_{n+1}^\dagger b_n + b_n^\dagger b_{n+1}) + eER(a_n^\dagger b_n + b_n^\dagger a_n) \Big]. \quad (1)$$

The integers n label the lattice sites and the operators a and b refer to electrons in the two minibands; the first two terms give the (field-dependent) site energies, the next two describe site-to-site hopping, and the last one is the term responsible for the interminiband transfer. The overlap matrix element R is model dependent and may depend on time through its momentum argument; we take it as a constant corresponding to a Kronig-Penney model. At zero applied field (1) leads to two minibands, $\epsilon^{a,b}(k) = \Delta_0^{a,b} \mp (\Delta_1^{a,b}/2)\cos(kd)$, while at finite static fields the spectrum consists of two interpenetrating Wannier-Stark (WS) ladders [10]: $\epsilon_m^{a,b} = \Delta_0^a + eEdr^{a,b} - meEd$. The numbers $r^{a,b}(E)$ must be determined numerically, and results of such a calculation are shown in Fig. 1. It is important to notice that for certain field values the two levels come very close to each other; as we shall show below this leads to profound effects on Zener tunneling.

Let us next consider the equation of motion for the density matrix for a and b electrons. With accelerated Bloch states as the basis [11], the diagonal elements of the density matrix give the electron density at a k point following the semiclassical trajectory in reciprocal space, $k(t) = K - (e/\hbar)\int_0^t E(t')\,dt'$. We assume equilibrium at $t = 0$, when the density matrix is diagonal. Defining $\rho_\pm(K,t) = \rho_K^a(t) \pm \rho_K^b(t)$, we find the following equa-

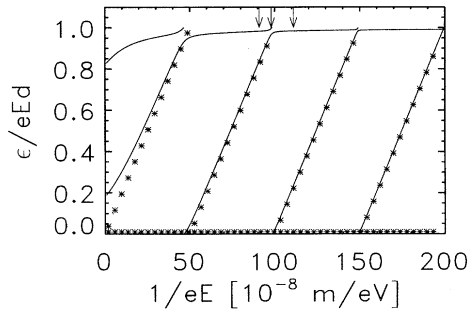

FIG. 1. Energy spectrum for a two-band superlattice as a function of applied dc field; continuous line corresponds to Eq. (1), while asterisks represent a model with no interminiband coupling ($R = 0$). The superlattice parameters are $d = 10$ nm, $\Delta_1^a = 0.8 \times 10^{-2}$ eV, $\Delta_1^b = 0.92 \times 10^{-2}$ eV, $\Delta^{ba} \equiv \Delta_0^b - \Delta_0^a = 2.0 \times 10^{-2}$ eV, and $R = -16d/9\pi^2$. The arrows indicate the three field strengths used in Fig. 2.

tions of motion [12]:

$$\dot{\rho}_+(K,t) = 0, \tag{2}$$

$$\dot{\rho}_-(K,t) = -Re\left\{h(K,t)\int_0^t dt'\, h^*(K,t')\rho_-(K,t')\right\}, \tag{3}$$

where

$$h(K,t) = 2\frac{e}{\hbar}E(t)R\exp\left[-\frac{i}{\hbar}\int_0^t \Delta\epsilon(k(t'))\,dt'\right] \equiv ue^{i\phi}. \tag{4}$$

In the above equations we have defined $\Delta\epsilon(k) = \epsilon^b(k) - \epsilon^a(k)$, and assumed that the intraminiband couplings are identical [13].

Equations (2)–(4) require several comments. If the interminiband coupling is turned off, they reduce to the normal collisionless Boltzmann equation (for two minibands), and thus contain, as special cases, the following standard results: (i) for static field one finds standard Bloch oscillations; and (ii) a harmonic E field leads to the above mentioned analog with Josephson effect, and, in particular, reproduces the band collapse discussed by Holthaus [4]. Note that only ρ_- is affected by interminiband transitions, while ρ_+, which fixes the particle density, is a constant of motion.

By differentiating the equation of motion for ρ_- with respect to time, one finds [12]

$$\ddot{\rho}_- - \frac{\dot{u}}{u}\dot{\rho}_- + u^2\rho_- + u\dot{\phi}\int_0^t dt'\frac{\dot{\phi}\dot{\rho}_-}{u} = 0. \tag{5}$$

Equation (5) forms the basis of our analysis, and the rest of this paper will describe the numerical results obtained from it under a number of specific physical conditions.

Steady fields.—In this case the dc field is turned on abruptly at $t = 0$. From Eq. (4) u is time independent, and Eq. (5) can be reduced to an ordinary third order differential equation:

$$\dot{\phi}\dddot{\rho}_- - \ddot{\phi}\ddot{\rho}_- + \dot{\phi}(u^2 + \dot{\phi}^2)\dot{\rho}_- - u^2\ddot{\phi}\rho_- = 0. \tag{6}$$

The accompanying initial conditions are $\rho_-(0) = \rho_-^0$, $\dot{\rho}_-(0) = 0$, and $\ddot{\rho}_-(0) = -u^2\rho_-(0)$. Thus, the initial values are determined by the miniband parameters, the k point in the Brillouin zone, and the temperature [which enters through $\rho_-(0)$]. From Eq. (5) it follows that $\rho_-(K,0)$ can be chosen equal to 1 without loss of generality.

Figure 2 displays a typical time dependence of ρ_-, obtained from Eq. (5) by numerical integration. One observes a very sensitive behavior with respect to variations of the applied field. For certain field values an "inversion" takes place: ρ_- reaches -1, which is the negative of its initial value, while for other nearby field values ρ_- stays close to its initial value. This behavior can be understood by examining Fig. 1: The two energy levels are very close to each other for certain electric field strengths, and in the corresponding neighborhoods a strongly enhanced band-to-band transfer takes place. This situation is quite different from what one expects from simple Zener tunneling theory [1]: there the tunneling rate is a monotonic function of the applied field [14]. The situation is summarized in Fig. 3, where we plot these Zener resonances as a function of the applied field. One can assign an index to the resonances: The resonance at the highest field (which corresponds approximately to aligning the levels at adjacent quantum wells) is called the first resonance, the next highest the second resonance (the case of Fig. 2), and so forth. Adopting this numbering scheme we observe that in the low field limit $E^{(n)} \approx \Delta^{ba}/ned$ (here $\Delta^{ba} = \Delta_0^b - \Delta_0^a$).

Further insight into the physical meaning of the various oscillations of Fig. 2 can be obtained by considering the Fourier transform of ρ_-. Let us first try to establish a qualitative picture of what to expect. The initial state of the system is described by some wave function, say,

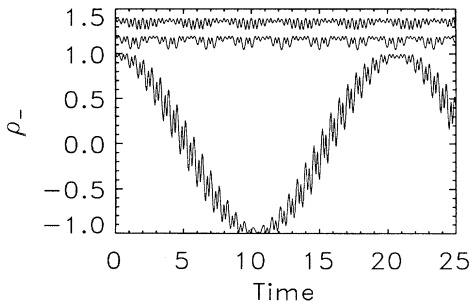

FIG. 2. Time dependence of $\rho_-(K = 0)$ for three different field values: top, $eE = 1.1 \times 10^6$; middle, 0.9×10^6; and bottom, 1.02×10^6 eV/m, respectively. For clarity, we have shifted the top and middle curve upwards by 0.4 and 0.2, respectively. The superlattice parameters are as in Fig. 1, and the unit on the time axis is $10^3\hbar/\text{eV} \simeq 4.14$ ps.

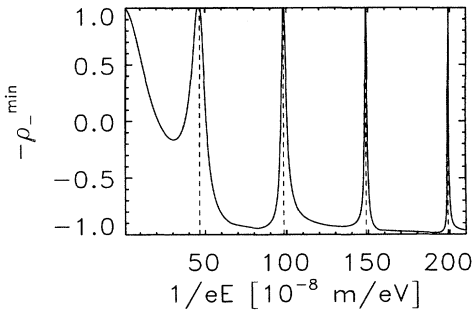

FIG. 3. The negative of $\rho_-^{\min}$ as a function of applied field. If $-\rho_-^{\min} \simeq 1$, a strong band-to-band transfer is taking place ("Zener resonance"). The dashed lines mark where the WS ladder separation has local minima.

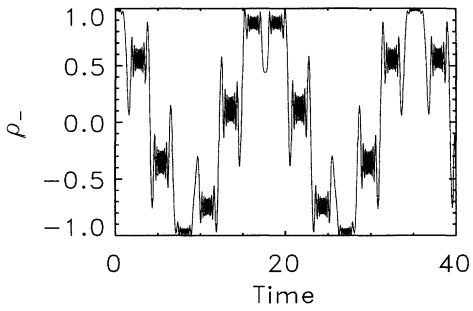

FIG. 5. Time dependence of $\rho_-(K = 0)$ for superlattice parameters $\Delta_1^a = \Delta_1^b = 1.8 \times 10^{-2}$ eV, $\Delta^{ba} = 2.0 \times 10^{-2}$ eV, and $R = -0.9d$. Units for the time axis are as in Fig. 2, and the field is $E = 0.232 \times 10^6$ V/m, corresponding to the eighth Zener resonance.

$|\Psi(0)\rangle$, which is not an eigenstate after the field has been turned on. However, it can be expanded in terms of the eigenstates: $|\Psi(0)\rangle = \sum_n c_n \psi_n^a + d_n \psi_n^b$. Since $\rho(t) = |\Psi(t)\rangle\langle\Psi(t)|$, and each eigenstate evolves according to $\psi_n^{a,b}(t) = \exp(-i\epsilon_n^{a,b}t)\psi_n^{a,b}$, large Fourier components in ρ_- are expected to occur at $\hbar\omega = meEd$ and $\hbar\omega = \pm eEd(r^a - r^b) + meEd$ [15]. This expectation is fully born out by the numerical evaluation of $\rho_-(\omega)$. Figure 4 shows the results of the two independent calculations: the continuous lines are obtained based on Fig. 1, while the asterisks come from the Fourier transform of $\rho_-(t)$. Naturally, the more laborious calculation based on $\rho_-(t)$ contains also more information: The *magnitudes* of the Fourier components (not shown in the figure) are needed in the evaluation of other physical quantities, such as the current, which will be addressed elsewhere [12].

It is also of interest to examine the effect of varying the superlattice parameters. Figure 5 shows the time dependence of $\rho_-(K = 0)$ when the field is tuned to the eighth Zener resonance and we have increased the bandwidths and interminiband coupling. A distinctive set of stable plateaus has developed. The transitions between

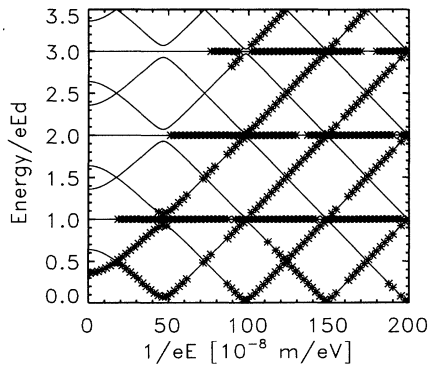

FIG. 4. Fourier spectrum of $\rho_-(K = 0, t)$. The most significant peaks in the Fourier spectrum are indicated by asterisks, and the continuous lines are energy differences between the interpenetrating WS ladders.

the plateaus occur at instants $t = \frac{1}{2}T_B, \frac{3}{2}T_B, \frac{5}{2}T_B, \ldots$ after the field was turned on. Thus, the lifetime of a plateau is (approximately) equal to the Bloch period, and transitions occur every time the k point reaches the Brillouin zone edge [16]. This behavior is generic to the *low field regime*, $E \leq \Delta^{ba}/ed$, and we can qualitatively understand features in the time dependence of $\rho_-(t)$ by considering the semiclassical motion of a k point between the extrema of the Brillouin zone; transitions to the other minibands occur mainly at zone edges, where the energy separation between the minibands is at a minimum.

We can also understand the *number* of oscillations on a given plateau by examining Eq. (5) under some simplifying assumptions. In particular, if we assume that $\Delta\epsilon$ has a weak time dependence, it is easy to solve (5) analytically. The solution suggests defining a "local" time dependent frequency for a general, but sufficiently slowly varying $\Delta\epsilon$ to be $\omega_l^2(t) = \omega_c^2 + \omega_d^2(k(t))$. Here $\omega_c = 2(|R|/d)\omega_B$ and $\hbar\omega_d(k) = \Delta\epsilon(k)$. Thus, in the low field limit we can identify the number of oscillations $N_{\rm osc} \equiv \langle\omega_l(t)\rangle/\omega_B = \Delta^{ba}/\hbar\omega_B$, where the time average was calculated over the Bloch period T_B. Consequently, at the nth Zener resonance, we find $N_{\rm osc} = n$. In Fig. 2 one can distinguish two periods of oscillation in any of the plateaus (even though the plateaus are not very clearly resolved for this particular set of parameters), while Fig. 5 clearly shows eight periods of oscillation within a plateau.

In the *high field regime*, $E > \Delta^{ba}/ed$, the situation differs drastically from semiclassical expectations: the plateaus vanish, and we find from Eq. (6), both numerically and analytically, that $\rho_-(t)$ oscillates between -1 and $+1$ with a single frequency ω_c.

Alternating fields.—In the case of a temporally periodic driving field one can make a close parallel to the treatment of a spatially periodic potential. Given a Hamiltonian with $H(t + T) = H(t)$, the starting point is Floquet's theorem applied to the Schrödinger equation. This gives wave functions of the form $\psi_\epsilon = \exp(-i\epsilon t)u_\epsilon(t)$, where $u_\epsilon(t + T) = u_\epsilon(t)$. We have

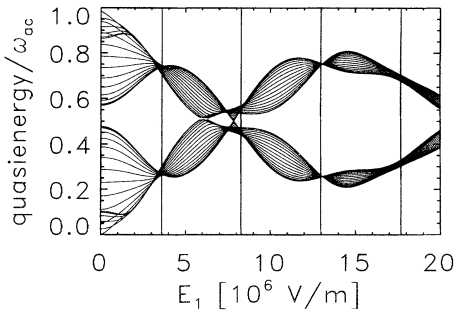

FIG. 6. Quasienergy spectrum for the superlattice of Fig. 1. We display the field dependence of 17 K points, which are evenly distributed in the positive half of the Brillouin zone, $K \in [0, \pi/d]$ (due to evenness of the quasienergy spectrum negative K's would be redundant). The vertical lines indicate where the band collapse would occur for noninteracting minibands. The modulation frequency is $\omega_{ac} = 1.5 \times 10^{-2}$ eV/$\hbar$.

introduced the *quasienergy* ϵ, which is defined modulo $\omega_{ac} = 2\pi/T$, leading in a natural way to the definition of a *quasienergy Brillouin zone*. The functions ψ_ϵ are eigenstates to $S = H - i\hbar\partial/\partial t$, i.e., they are given by the temporal Bloch theorem applied to S. These considerations have been employed by Holthaus [4] in his analysis of the one-miniband case, and we now wish to extend these concepts to two minibands in the context of the Hamiltonian (1). The quasienergy spectrum for an applied field of the form $E(t) = E_1 \cos \omega_{ac} t$ is shown in Fig. 6 [17]. For vanishing band coupling the band collapses occur whenever $eE_1 d/\hbar\omega_{ac}$ equals a root of the zeroth Bessel function, and we observe that the two-band model displays strict band collapse at only one of these roots. However, there is a clear tendency towards bandwidth narrowing at the other roots.

The next step in the analysis is to solve the equation of motion for $\rho_-(K, t)$ for the time dependent case. One can perform a construction as in Fig. 4; now the quasienergy differences (modulo ω_{ac}) correspond to the leading Fourier components of $\rho_-(K, \omega)$. Since the quasienergy differences depend on K (see Fig. 6), the construction of Fig. 4 must be done separately for each K. Just as in the static case we can relate the various features in the time dependence of $\rho_-(K, t)$ to the details of the quasienergy spectrum of Fig. 6. The detailed analysis is postponed to our full paper [12], but here we point out that in the low field limit, $E_1 < \hbar\omega_{ac}/ed$, the interminiband tunneling is quenched, and the time dependence is described by the semiclassical equations of motion.

Let us comment on the experimental possibilities of observing the phenomena predicted in this work. While the full inversion of ρ_- requires coherence time scales of tens of picoseconds, which is large by present experimental standards, many other aspects, such as the plateaus, occur on a much shorter time scale, and should therefore be more easily detected. Further, by optimizing the superlattice parameters it is possible to obtain more favorable conditions for experiments.

In summary, we have presented a time-dependent formulation of transport in superlattices. We have found that the dynamics of the two-band model can show, in addition to conventional Bloch oscillations, significant additional structure: Zener resonances, stable plateaus, and band collapses.

[1] F. Bloch, Z. Phys. **52**, 555 (1928); C. Zener, Proc. R. Soc. London A **145**, 523 (1934).
[2] L. Esaki and R. Tsu, IBM J. Res. Dev. **14**, 61 (1970).
[3] C. Waschke *et al.*, Phys. Rev. Lett. **70**, 3318 (1993).
[4] M. Holthaus, Phys. Rev. Lett. **69**, 351 (1992); Z. Phys. B **89**, 251 (1992).
[5] P. S. S. Guimarães *et al.*, Phys. Rev. Lett. **70**, 3792 (1993).
[6] A. A. Ignatov and Y. A. Romanov, Phys. Status Solidi (b) **73**, 327 (1976); D. H. Dunlap and V. M. Kenkre, Phys. Rev. B **34**, 3625 (1986).
[7] M. Büttiker *et al.*, Phys. Lett. **96A**, 365 (1983); A. A. Ignatov *et al.*, Phys. Rev. Lett. **70**, 1996 (1993).
[8] T. Meier *et al.*, Phys. Rev. Lett. **73**, 902 (1994).
[9] See, however, D. W. Hone and M. Holthaus, Phys. Rev. B **48**, 15 123 (1993); **49**, 16 605 (1994), where a finite multiband superlattice in an ac field is discussed.
[10] H. Fukuyama *et al.*, Phys. Rev. B **8**, 5579 (1973); D. Emin and C. F. Hart, Phys. Rev. B **36**, 7353 (1987).
[11] J. B. Krieger and G. J. Iafrate, Phys. Rev. B **33**, 5394 (1986); **35**, 9644 (1987); **38**, 6324 (1988).
[12] J. Rotvig, A. P. Jauho, and H. Smith (unpublished).
[13] Explicitly, we assume that $R_{11} = R_{22}$, where $R_{nn}(k) = (i/d) \int_{-d/2}^{d/2} dx\, u_{n,k}^*(x) \nabla_k u_{n,k}(x)$. This assumption is valid, e.g., for the Kronig-Penney model.
[14] Nonexponential corrections to Zener tunneling were found by P. Ao and J. Rammer, Phys. Rev. B **43**, 5393 (1991), and perturbative analyses of resonances have been carried out in Ref. [11] and by K. Mullen *et al.*, Phys. Rev. B **47**, 2689 (1993).
[15] Here we used the known energy spectrum of the biased superlattice [10]. Observe also that the *slowest* frequency is determined by the *minimal* distance of the energy levels. It is easily verified from Figs. 1 and 2 that this is indeed the case.
[16] Since $K = 0$ in Fig. 5, which corresponds to the center of the Brillouin zone, the first transition occurs at $t = T_B/2$.
[17] We apply the method suggested by X.-G. Zhao *et al.* (unpublished), and use the variable K to label the states.